NANO LETTERS

pubs.acs.org/NanoLett Letter

# Quantifying Strain in Moiré Superlattice

Jiamin Quan,[#] Ganbin Chen,[#] Lukas Linhart, Zhida Liu, Takashi Taniguchi, Kenji Watanabe, Florian Libisch, Rui Huang,* and Xiaoqin Li*

Cite This: *Nano Lett.* 2023, 23, 11510−11516 Read Online

ACCESS | Metrics & More | Article Recommendations | Supporting Information

**ABSTRACT:** In twisted van der Waals (vdW) bilayers, intrinsic strain associated with the moiré superlattice and unintentionally introduced uniaxial strain may be present simultaneously. Both strains are able to lift the degeneracy of the $E_{2g}$ phonon modes in Raman spectra. Because of the different rotation symmetry of the two types of strain, the corresponding Raman intensity exhibits a distinct polarization dependence. We compare a 2.5° twisted $MoS_2$ bilayer, in which the maximal intrinsic moiré strain is anticipated, and a natural $MoS_2$ bilayer with an intentionally introduced uniaxial strain. By analyzing the frequency shift of the $E_{2g}$ doublet and their polarization dependence, we can not only determine the direction of unintentional uniaxial strain in the twisted bilayer but also quantify both strain components. This simple strain characterization method based on far-field Raman spectra will facilitate the studies of electronic properties of moiré superlattices under the influence of combined intrinsic and external strains.

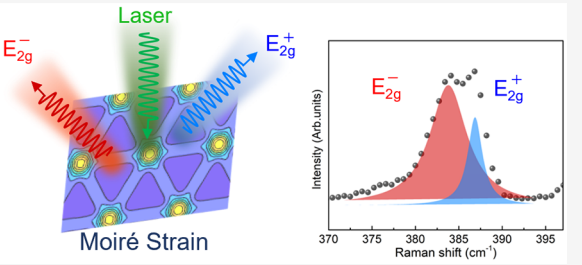


**KEYWORDS:** *van der Waals materials, Moiré superlattice, Atomic reconstruction, Raman spectroscopy, Strain*



Strain engineering plays a key role in tuning the properties of epitaxial materials in general.[1] In atomically thin van der Waals (vdW) materials, strain tuning can be particularly effective because these materials are often mechanically strong and highly sensitive to external stimuli (e.g., electric field and doping),[2,3] including strain. In the case of transition metal dichalcogenides (TMDs), strain engineering has been applied to modify band gaps[4] and valley polarization,[5] to induce the exciton valley Hall effect,[6] to engineer phonon dispersion,[7−9] and to define locations of quantum emitters.[10−12] An exciting development in the field of vdW quantum materials is the realization that moiré superlattices (MSLs) can be used as a versatile platform to realize correlated electronic phases[13−15] and photonic functionalities.[16] Formed by vertically stacking two thin layers with either different lattice constants or a precisely controlled twist angle, a periodic pattern of atomic alignment between the two layers leads to in-plane supercells of sizes ranging from a few nanometers to a few micrometers.[17−19] In mechanically stacked MSLs, extrinsic and intrinsic moiré strains may coexist and cause different modifications to electronic bands and phonon properties.[20]

Here, we establish a method for quantifying both intrinsic and extrinsic strains in a twisted $MoS_2$ bilayer. We use polarization resolved Raman spectroscopy to characterize strain in a series of twisted $MoS_2$ bilayers prepared with a standard tear-and-stack method that allows the twist angle to be controlled with an accuracy better than 0.1°.[21] The 2-fold degenerate $E_{2g}$ mode splits into a $E_{2g}^+$ and $E_{2g}^-$ doublet, which can be used to quantify the strain. The distinction between the intrinsic moiré strain and an extrinsic uniaxial strain introduced unintentionally in the bilayer is reflected in the polarization dependence of the Raman intensity. Due to the 3-fold symmetry in MSLs assembled from two hexagonal monolayers, the intrinsic moiré strain possesses the same 3-fold symmetry. Correspondingly, the intensity of the $E_{2g}$ doublet is isotropic; i.e., it does not change with the polarization of an analyzer in the detection path. In contrast, an extrinsic uniaxial strain stretches a bilayer in a particular direction, leading to a 2-fold symmetry and anisotropy in the polarization-dependent intensity of the $E_{2g}$ modes.[22,23] By fitting the split $E_{2g}$ modes and their polarization patterns, we can quantify both types of strain and determine the direction of the extrinsic uniaxial strain. Because of the relative simplicity of the far-field Raman measurements, this approach is broadly applicable to evaluate strain in vdW bilayers with ∼1 $\mu$m spatial resolution, thus providing a convenient characterization method useful for guiding strain engineering of vdW materials in general.

Because of the varying interlayer coupling and strain at different twist angles, the evolution of the lattice reconstruction at small twist angles can be categorized into three different regimes.[24] In TMD homobilayers, such as $MoS_2$, there is a substantial lattice reconstruction in a surprisingly large range of

**Received:** August 21, 2023
**Revised:** December 6, 2023
**Accepted:** December 7, 2023
**Published:** December 12, 2023

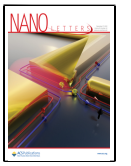

twist angles. In the relaxed regime ($0° < \theta < 2°$), triangular domains with the energetically favorable AB (BA) stacking (or 3R stacking)[25,26] are separated by sharp domain walls with energetically unfavorable AA stacking sites as topological defects.[27] Beyond $\theta = 2°$, the MSL enters the transition regime, where the boundary between the domains becomes blurry. Finally, the twisted bilayer reaches the rigid regime at large twist angles ($\theta \geq 6°$) with minimal lattice distortion in each layer.[26,28] In the following, we focus on a $MoS_2$ bilayer with a twist angle $\theta = 2.5°$, where the intrinsic moiré strain is close to its maximum according to our previous study.[24] In the Supporting Information, we include measurements from a series of twist bilayers with twist angles ranging from 0° to 20° to demonstrate a systematic evolution of intrinsic moiré strain as manifested in Raman spectra.

Without considering lattice relaxation, the local atomic stacking in an MSL is determined by rotating pristine two-dimensional (2D) lattices. In the case of a 2.5° twisted $MoS_2$ bilayer, a hexagonal superlattice pattern forms (see Figure 1a).

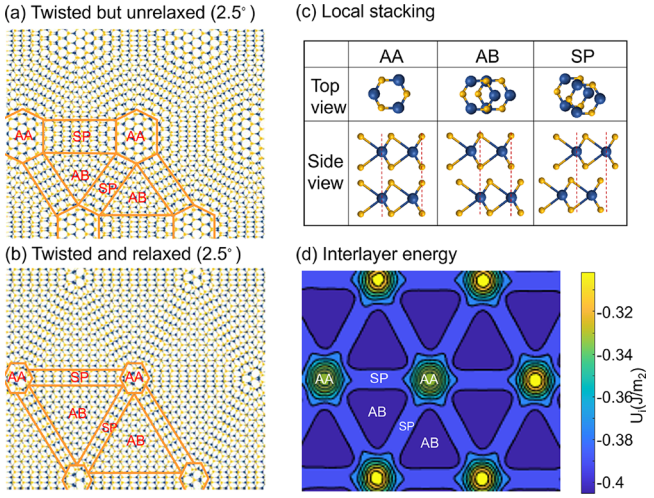


**Figure 1.** Atomic reconstruction of moiré superlattice in $MoS_2$ twisted bilayers. (a) Schematics of atomic stacking of rigid lattices with a twist angle of 2.5°. (b) Relaxed moiré superlattice with a twist angle of 2.5°. Local atomic alignments are shown at three locations, corresponding to a topological defect (AA), a domain center (AB), and a domain wall or saddle point (SP). (c) Schematic diagrams of local high-symmetry stacking configurations. AB and BA stackings are equivalent except for an inversion along the $z$ direction. For AB (BA) stacking, S (Mo) atoms are directly on top of Mo (S) atoms, and the other Mo and S atoms are at the center of the hexagon. For AA stacking, all Mo (S) atoms of one layer are directly on top of Mo (S) atoms of the other layer. For SP stacking, it is an intermediate configuration between AB and BA stacking. This arrangement is characterized by the alignment of all the S atoms and also all the Mo atoms in the armchair direction, as indicated in the top view. (d) Distribution of the interlayer energy corresponding to the relaxed moiré superlattice with a twist angle of 2.5°.

However, driven by the relatively strong interlayer coupling at small twist angles,[26,29,30] the twisted bilayer reconstructs to reduce the interlayer stacking fault energy while incurring a penalty of strain and a corresponding increase in the strain energy. The lattice reconstruction minimizes the sum of the interlayer energy and the strain energy, resulting in a regular triangular pattern with three distinct types of local high-symmetry stacking configurations: AA, AB (BA), and domain walls (saddle point, SP) that separate the AB and BA regions (see Figure 1b, c). After lattice reconstruction, the distribution of the interlayer energy exhibits a triangular pattern (Figure 1d) similar to that calculated via a continuum model (see section III in the Supporting Information).

The lattice reconstruction induces a spatial distribution of shear strain in the twisted bilayer, as shown in Figure 2a for a

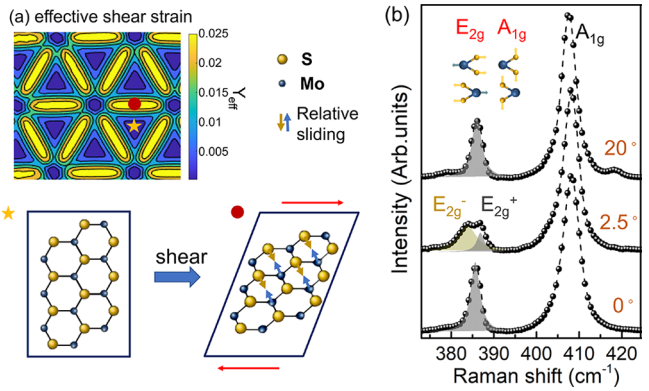


**Figure 2.** Shear strain in a moiré superlattice leading to splitting of the $E_{2g}$ phonon. (a) The effective shear strain distribution in a moiré superlattice formed by a $MoS_2$ bilayer with a twist angle of 2.5° (upper panel). Top view of an unstrained $MoS_2$ monolayer (lower left panel) and the distorted $MoS_2$ lattice under a shear strain (lower right panel). The lower panels illustrate lattices at two locations: a red circle along the domain wall and a yellow star at the center of a domain. Arrows show the relative displacements of Mo and S atoms. (b) Representative Raman spectra measured from $MoS_2$ bilayers with different twist angles: 0, 2.5, and 20°. The $E_{2g}$ mode splitting is clearly observed from the bilayer with a twist angle of 2.5°. Atomic motions corresponding to two phonon modes $A_1g$ and $E_{2g}$ are illustrated as an inset.

2.5° twisted $MoS_2$ bilayer calculated by using the continuum model. Closer examination of the local atomic structure reveals conserved hexagonal symmetry of the $MoS_2$ lattice in the AA and AB domains without shear strain (marked by a yellow star in Figure 2a), while the hexagons become distorted at the domain walls due to shear strain (marked by a red circle, Figure 2a). In the distorted lattice structure, shear strain breaks the hexagonal symmetry with lattice elongation in one of the armchair directions and simultaneous lattice contraction in the perpendicular zigzag direction (Figure 2a).

Raman spectroscopy is an effective technique for probing symmetries and strain in 2D materials, particularly through the 2-fold degenerate $E_{2g}$ mode.[4,7,31] In the presence of a 2D strain tensor $\varepsilon_{ij}$ the 2D secular equation for Raman spectra takes the form

$$\begin{vmatrix} p\varepsilon_{xx} + q\varepsilon_{yy} - \lambda & 2r\varepsilon_{xy} \\ 2r\varepsilon_{xy} & p\varepsilon_{yy} + q\varepsilon_{xx} - \lambda \end{vmatrix} = 0 \quad (1)$$

where $(p, q, r)$ are three components of the phonon deformation potential, $\lambda = \omega^2 - \omega_0^2 \approx 2\omega_0\Delta\omega$, $\omega_0$ is the frequency of the optical phonons in the absence of strain, and $\Delta\omega$ is the frequency shift.[32] Solving eq 1, we obtain two eigenvalues and the corresponding frequency shifts:


https://doi.org/10.1021/acs.nanolett.3c03115
Nano Lett. 2023, 23, 11510−11516

$$\Delta\omega_{1,2} = \frac{\lambda_{1,2}}{2\omega_0} = \frac{1}{2\omega_0}\left[\frac{p+q}{2}(\varepsilon_{xx}+\varepsilon_{yy}) \pm \sqrt{\left(\frac{p-q}{2}\right)^2(\varepsilon_{xx}-\varepsilon_{yy})^2+4r^2\varepsilon_{xy}^2}\right] \quad (2)$$

Due to the $D_{3h}$ symmetry of the $MoS_2$ monolayer, the frequency shifts under a pure shear strain ($\varepsilon_{xy} = \varepsilon$, $\varepsilon_{xx} = \varepsilon_{yy} = 0$) are equivalent to those under a biaxial strain of equal and opposite components ($\varepsilon_{xx} = \varepsilon$, $\varepsilon_{yy} = -\varepsilon$, $\varepsilon_{xy} = 0$). Thus, we must have $2r = p - q$, and there are only two independent components of the phonon deformation potential in 2D. With this relation, the frequency shifts can be rewritten as

$$\Delta\omega_{1,2} = \frac{p+q}{2\omega_0}\varepsilon_m \pm \frac{p-q}{4\omega_0}\gamma_{eff} \quad (3)$$

where $\varepsilon_m = (\varepsilon_{xx} + \varepsilon_{yy})/2$ is the 2D mean strain, and $\gamma_{eff} = \sqrt{(\varepsilon_{xx}-\varepsilon_{yy})^2+4\varepsilon_{xy}^2}$ is the effective shear strain in 2D. Correspondingly, the Grüneisen parameter and the shear deformation potential are

$$\alpha = -\frac{1}{2\omega_0}\frac{\partial\omega}{\partial\varepsilon_m} = -\frac{p+q}{4\omega_0^2} \quad (4)$$

$$\beta = \frac{2}{\omega_0}\left|\frac{\partial\omega}{\partial\gamma_{eff}}\right| = \frac{|p-q|}{2\omega_0^2} \quad (5)$$

Thus, the frequency shifts in terms of the Grüneisen parameter and the shear deformation potential are

$$\Delta\omega_{1,2} = -2\omega_0\alpha\varepsilon_m \pm \frac{1}{2}\omega_0\beta\gamma_{eff} \quad (6)$$

Based on eq 6, we anticipate that the $E_{2g}$ peak splits into a doublet once the intrinsic shear strain in the twisted bilayer reaches a certain magnitude. To experimentally probe and understand the intrinsic moiré strain through $E_{2g}$ modes, the high-frequency Raman spectra from samples with twist angles of 0, 2.5, and 20° are shown in Figure 2b. Two dominant Raman modes in $MoS_2$ are attributed to the $E_{2g}$ and $A_{1g}$ modes[33] that correspond to in-plane and out-of-plane atomic motions as illustrated in the inset of Figure 2b. While the $A_{1g}$ mode exhibits only a slight shift as a function of the twist angle, the $E_{2g}$ mode undergoes a significant change. The $E_{2g}$ mode exhibits a single resonance with a narrow line width in both the 0 and 20° bilayers. In contrast, the $E_{2g}$ mode in the 2.5° bilayer splits into a doublet, $E_{2g}^+$ and $E_{2g}^-$. By fitting the data with two Lorentzian functions, the splitting is extracted to be 3.2 ± 0.2 $cm^{-1}$, which indicates a sizable moiré strain in this bilayer. We also include measurements from another sample with nominally the same twist angle $\theta = 2.5°$ to demonstrate the reproducibility (section V in the Supporting Information).

A natural question arises: how does one disentangle splittings due to intrinsic moiré strain caused by lattice reconstructions from an extrinsic strain often unintentionally applied to the bilayer? The key difference lies in the symmetry of the strain distribution. Due to the 3-fold symmetry in a MSL, Raman spectra taken over a laser spot of diameter ~1 μm would average over multiple supercells with domain walls oriented along three different directions, leading to an isotropic intensity of the $E_{2g}$ mode. By contrast, an additional, extrinsic uniaxial strain in the 2.5° twisted bilayer results in an anisotropic polarization-dependent intensity of the $E_{2g}$ modes. The domains are smaller than the laser spot size. While we anticipate some variations of the strain between different domains, such variations are likely smooth and gradual. We confirm the sample's spatial uniformity by taking the Raman intensity map of low-frequency shear and breathing modes (section VI in the Supporting Information).

A series of polarization-resolved Raman spectra are taken on both the 2.5° twisted bilayer and a natural bilayer with an intentionally introduced uniaxial strain, as shown in Figure 3.

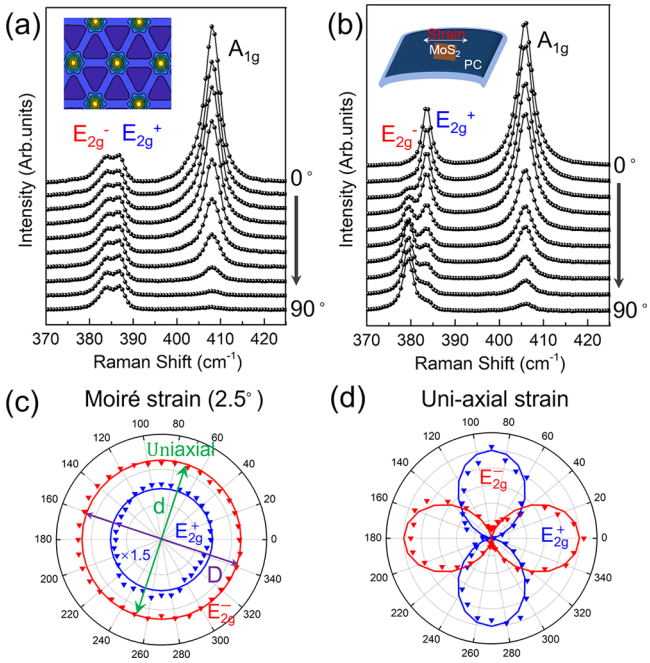


**Figure 3.** Comparison between polarization-resolved Raman spectra taken from a $MoS_2$ twisted bilayer with a twist angle of 2.5° and a natural $MoS_2$ bilayer subject to an externally applied uniaxial strain. Raman spectra when a polarizer in the path of the incident light is rotated from colinear to cross-linear polarization w.r.t. the analyzer polarization measured from (a) the 2.5° twisted bilayer and (b) the natural bilayer subject to an external uniaxial strain. The spectra are collected every 10°. The insets illustrate the main method of introducing strain via (a) intrinsic moiré and (b) uniaxial mechanical strain, respectively (additional details in the Supporting Information). Normalized polar plots of spilt $E_{2g}$ modes from (c) the 2.5° twisted bilayer and (d) the strained natural bilayer.

In the 2.5° bilayer, the intensity of the $A_{1g}$ mode shows a drastic change with incident light polarization, owing to its scalar matrix of Raman tensor.[22,23] In contrast, there are only minimal intensity changes observed for the $E_{2g}$ doublet (Figure 3c, d). Since the $E_{2g}$ doublet reacts more sensitively to strain, we extract the intensities of the $E_{2g}^+$ and $E_{2g}^-$ contributions as a function of incident light polarization (Figure 3c, d). The polar plot features an elliptical shape with a long ($D$) and a short ($d$) axis. In the case of a natural bilayer with an intentionally applied uniaxial strain, the lattice is elongated along a specific direction. Polarization-resolved Raman spectra, taken on such a strained bilayer, were subjected to a uniaxial strain of 1.4% (see section I in the Supporting Information), and they exhibit clear 2-fold symmetry in the intensity of both the $E_{2g}^+$ and $E_{2g}^-$ modes


https://doi.org/10.1021/acs.nanolett.3c03115
Nano Lett. 2023, 23, 11510−11516

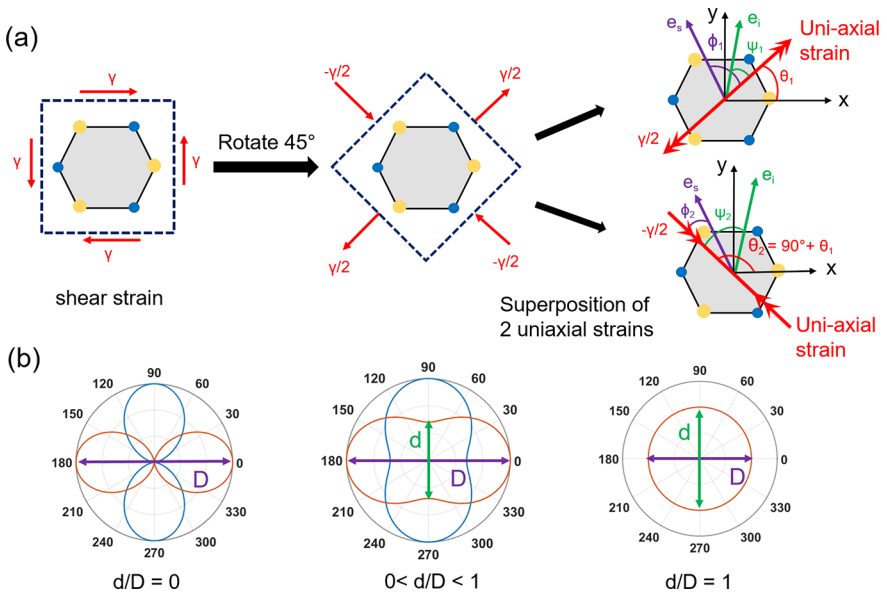


**Figure 4.** Strain analysis based on polar-Raman spectra. (a) The shear strain in a twisted bilayer is equivalent to a biaxial strain of equal and opposite components in the 45° rotated directions, treated as a superposition of two uniaxial strains in perpendicular directions. Here, $\gamma$ represents the shear strain. The polarization of the incident and scattered lights, represented by vectors $e_i$ and $e_s$, deviate from the strain directions by angles $\psi_1$ and $\psi_2$, and $\phi_1$ and $\phi_2$, respectively. (b) Polar-Raman plots of different strain states: a uniaxial strain (left), superposition of a shear strain and a uniaxial strain (middle), and a shear strain (right). The symbols $d$ and $D$ represent the short and long axes, respectively, of the polar plot.

(Figure 3d). The intensity of the $E^+_{2g}$ mode becomes maximal (minimal) when the polarization of incident light is parallel (perpendicular) to the direction of uniaxial strain.

The distinct polarization patterns between the uniaxial strain and the intrinsic moiré strain allow us to disentangle different types of strain in the twisted bilayers. Evidently, the evolution of the $E_{2g}$ modes with polarization direction (Figure 3c) shows that the intensity of the $E_{2g}$ modes is not strictly isotropic, suggesting that an additional extrinsic strain coexists with the intrinsic moiré strain. To quantify both strains in the twisted $MoS_2$ bilayers, we first consider a twisted bilayer with no extrinsic strain. In this idealized case, the shear strain dominates ($\gamma$), as illustrated in the left panel of Figure 4a. The shear strain is equivalent to a biaxial strain of equal and opposite components if we rotate the reference coordinates by 45° (the middle panel of Figure 4a). The biaxial strain can be treated as a superposition of two mutually perpendicular uniaxial strains (right panel of Figure 4a). This superposition can be observed in the polarization-resolved Raman spectra. Therefore, the polarization dependence in the case of shear strain can be determined by superimposing the polarization dependence due to two mutually perpendicular uniaxial strains. The upper right panel of Figure 4a shows a hexagonal lattice under a uniaxial tensile strain ($\varepsilon_1 = \gamma/2$) at an angle $\theta_1$ with respect to the $x$-axis, while the lower right panel shows the lattice under a uniaxial compressive strain ($\varepsilon_2 = -\gamma/2$) at an angle $\theta_2 = \theta_1 + 90°$ with respect to the $x$-axis. The polarizations of the incident and scattered light are represented by vectors $e_i$ and $e_s$, respectively, with the angles between $e_i$ ($e_s$) and the uniaxial strain directions denoted by $\psi_1$ and $\psi_2$ ($\phi_1$ and $\phi_2$).

Each uniaxial strain leads to a polarization-dependent intensity of the $E_{2g}$ modes:[23]

$$I_{E^+_{2g}}(\varepsilon) \propto {d_0}^2 \cos^2(\phi + \psi + 3\theta) \tag{7}$$

$$I_{E^-_{2g}}(\varepsilon) \propto {d_0}^2 \sin^2(\phi + \psi + 3\theta) \tag{8}$$

where $\theta$ is the angle between the direction of the uniaxial strain and the $x$-axis and $\psi$ ($\phi$) is the angle between $e_i$ ($e_s$) and the uniaxial strain, and $d_0$ represents the magnitude of the intensity due to the uniaxial strain.

By superimposing the intensities of the $E_{2g}$ modes due to the two mutually perpendicular uniaxial strains ($\varepsilon_1 = \gamma/2$ and $\varepsilon_2 = -\gamma/2$), we obtain the intensities due to the equivalent shear strain as

$$I_{E^+_{2g}}(\gamma) = I_{E^+_{2g}}(\varepsilon_1) + I_{E^+_{2g}}(\varepsilon_2) \propto {d_0}^2 \tag{9}$$

$$I_{E^-_{2g}}(\gamma) = I_{E^-_{2g}}(\varepsilon_1) + I_{E^-_{2g}}(\varepsilon_2) \propto {d_0}^2 \tag{10}$$

which exhibit no polarization dependence for either mode. Therefore, the intrinsic shear strain in the twisted bilayer would lead to an isotropic Raman intensity for the $E_{2g}$ modes.

Next we consider a $MoS_2$ bilayer combining both extrinsic uniaxial and intrinsic moiré strains. The intensities of the $E_{2g}$ modes are obtained by superposition as

$$I_{E^+_{2g}} = I_{E^+_{2g}}(\gamma) + I_{E^+_{2g}}(\varepsilon) \propto d_\gamma^2 + d_\varepsilon^2 \cos^2(\phi + \psi + 3\theta_0) \tag{11}$$

$$I_{E^-_{2g}} = I_{E^-_{2g}}(\gamma) + I_{E^-_{2g}}(\varepsilon) \propto d_\gamma^2 + d_\varepsilon^2 \sin^2(\phi + \psi + 3\theta_0) \tag{12}$$

where $d_\gamma^2$ and $d_\varepsilon^2$ represent the magnitudes of the intensity due to the intrinsic shear strain ($\gamma$) and uniaxial strain ($\varepsilon$), respectively. $\theta_0$ is the angle between the direction of the uniaxial strain and the $x$-axis. Since the polarization-dependent Raman spectra reflect a combination of the intrinsic shear strain due to twist and the unintentionally introduced uniaxial strain, the ratio between the short and long axes of the polar plot ($d/D$) characterizes the ratio between the intensities due to the two types of strain. In Figure 4b, the left panel represents the case of a uniaxial strain ($\gamma = 0$, $d/D = 0$), and the right panel represents the case of an intrinsic shear strain ($\varepsilon = 0$, $d/D = 1$). The middle panel represents an intermediate case


https://doi.org/10.1021/acs.nanolett.3c03115
Nano Lett. 2023, 23, 11510−11516

when the twisted bilayer is under combined shear (intrinsic) and uniaxial strains ($0 < d/D < 1$). From the measured polarization dependence in Figure 3c, we obtain a fitted $d/D$ value of 0.91, which indicates that the 2.5° bilayer is primarily subject to an intrinsic shear strain with a small unintentional uniaxial strain contribution.

Examining the polarization dependent intensities of the two $E_{2g}$ modes (Figure 3c) it is possible to extract both the direction and the magnitude of the uniaxial strain in a moiré superlattice. The direction of the uniaxial strain corresponds to the long (short) axis in the polar plot of the $E_{2g}^{+}$ ($E_{2g}^{-}$) mode. As shown in Figure 3c for the 2.5° twisted $MoS_2$ sample, the short axis for the $E_{2g}^{-}$ mode lies in the direction with an angle of ~70° from the $x$-axis, which reveals the direction of an unintentional uniaxial strain in the twisted bilayer.

To further quantify the uniaxial strain in the 2.5° twisted $MoS_2$ sample, we calculate the mean strain and the effective shear strain using the measured frequency shifts for the $E_{2g}$ modes (Figure 2b). Based on eq 6, we obtain

$$\varepsilon_m = -\frac{\Delta\omega_1 + \Delta\omega_2}{4\omega_0\alpha} \tag{13}$$

and

$$\gamma_{eff} = \frac{\Delta\omega_1 - \Delta\omega_2}{\omega_0\beta} \tag{14}$$

We take the Grüneisen parameter $\alpha = 1.1$ and the shear deformation potential $\beta = 0.78$ for $MoS_2$ based on previous studies.[22] The presence of a single $E_{2g}$ peak in the 0° sample suggests that the strain in this sample is minimal if any. Therefore, we take $\omega_0 = 384.7\ cm^{-1}$ from this single $E_{2g}$ peak. For the 2.5° twisted $MoS_2$ sample, the frequency shifts of the doublet are $\Delta\omega_{1,2} = 0.78$ and $-2.37\ cm^{-1}$. Then, using eqs 13 and 14, we obtain the mean strain $\varepsilon_m = 0.00094$ and the effective shear strain $\gamma_{eff} = 0.0105$.

Since the mean strain due to the intrinsic shear strain vanishes, the nonzero contribution must result from the presence of an extrinsic uniaxial strain as revealed by the elliptic polar plot. The magnitude of this uniaxial strain is thus estimated as $\varepsilon_u = 2\varepsilon_m = 0.0019$ (or 0.19%). The effective shear strain $\gamma_{eff}$ includes contributions from both the uniaxial strain and the intrinsic moiré strain. If we assume a simple superposition of the two effective shear strains, we obtain the intrinsic moiré strain as $\gamma_{moire} = \gamma_{eff} - \varepsilon_u = 0.0086$ (or 0.86%). The value of the intrinsic moiré strain agrees well with our numerical calculations ($\gamma_n = 0.88\%$; see section III in the Supporting Information). While the magnitude of the uniaxial strain is small compared to the intrinsic moiré strain, its presence is clearly observable in the polarization dependent intensities of the $E_{2g}$ modes (Figure 3c). Remarkably, the ratio between the short and long axes of the polar plot can be correlated with the relative magnitudes of strain as $d/D \approx \sqrt{1 - 2\varepsilon_m/\gamma_{eff}}$, for the 2.5° twisted $MoS_2$ sample as well as the two theoretical limits with $d/D = 0$ and 1 for a uniaxial strain and a pure shear strain, respectively.

In summary, we demonstrated that the polarization-resolved Raman spectra of $E_{2g}$ modes can be used to quantitatively assess both the intrinsic moiré strain and an unintentionally introduced uniaxial strain in a twisted $MoS_2$ bilayer. Both types of strain locally break the hexagonal symmetry of the crystal, causing a splitting of the $E_{2g}$ mode. By analyzing the polarization dependence and the frequency shift of the $E_{2g}$ doublet relative to the 0° sample, one can thus disentangle and quantify both the intrinsic moiré strain and the extrinsic uniaxial strain that may vary from sample to sample. Within the Raman spot size, the different directions of the intrinsic moiré strain average out, yielding an isotropic signal, while uniaxial strain features a clear directional dependence. Such a quantitative strain characterization method enables effective control of the rich ground states of MSLs including superconductivity and correlated insulator states.[20,34,35]

## ■ ASSOCIATED CONTENT

### Supporting Information

The Supporting Information is available free of charge at https://pubs.acs.org/doi/10.1021/acs.nanolett.3c03115.

Sample preparation, Raman measurement, continuum model and calculation, the measured Raman spectra as a function of twist angle, the Raman spectrum from another sample of 2.5°, and low-frequency Raman mapping (PDF)

## ■ AUTHOR INFORMATION


### Corresponding Authors

**Rui Huang** − *Department of Aerospace Engineering and Engineering Mechanics, The University of Texas at Austin, Austin, Texas 78712, United States*; Email: ruihuang@mail.utexas.edu

**Xiaoqin Li** − *Department of Physics, The University of Texas at Austin, Austin, Texas 78712, United States*; orcid.org/0000-0002-2279-3078; Email: elaineli@physics.utexas.edu

### Authors

**Jiamin Quan** − *Department of Physics, The University of Texas at Austin, Austin, Texas 78712, United States*

**Ganbin Chen** − *Department of Aerospace Engineering and Engineering Mechanics, The University of Texas at Austin, Austin, Texas 78712, United States*

**Lukas Linhart** − *Institute for Theoretical Physics, Vienna University of Technology, 1040 Vienna, Austria*

**Zhida Liu** − *Department of Physics, The University of Texas at Austin, Austin, Texas 78712, United States*

**Takashi Taniguchi** − *Research Center for Materials Nanoarchitectonics, National Institute for Materials Science, Tsukuba 305-0044, Japan*; orcid.org/0000-0002-1467-3105

**Kenji Watanabe** − *Research Center for Electronic and Optical Materials, National Institute for Materials Science, Tsukuba 305-0044, Japan*; orcid.org/0000-0003-3701-8119

**Florian Libisch** − *Institute for Theoretical Physics, Vienna University of Technology, 1040 Vienna, Austria*; orcid.org/0000-0001-5641-9458

Complete contact information is available at: https://pubs.acs.org/10.1021/acs.nanolett.3c03115

### Author Contributions

#J.Q. and G.C. contributed equally.


### Author Contributions

J.Q. prepared the TBL samples and led the optical experiments. G.C. led the theoretical calculations, and L.L. assisted with the theoretical discussions. T.T. and K.W. provided the hBN sample. J.Q., G.C., R.H., and X.L. wrote the manuscript. X.L., R.H., and F.L. supervised the project. All authors discussed the results.



https://doi.org/10.1021/acs.nanolett.3c03115
Nano Lett. 2023, 23, 11510−11516

### Notes

The authors declare no competing financial interest.

## ■ ACKNOWLEDGMENTS

The spectroscopy experiments at the University of Texas at Austin were primarily funded by the US Department of Energy, Office of Basic Energy Sciences, under grant DE-SC0019398 (J.Q.), NSF ECCS-2130552 (Z. L.) and a grant from the University of Texas. Material preparation was funded by the Welch Foundation via grant F-1662. G.C. and R.H. acknowledge the support of the National Science Foundation (CMMI 2225519). K.W. and T.T. acknowledge support from the JSPS KAKENHI (Grant Numbers 21H05233 and 23H02052) and World Premier International Research Center Initiative (WPI), MEXT, Japan. F.L. acknowledges support from COST Action 18234.

## ■ REFERENCES

(1) Ederer, C.; Spaldin, N. A. Effect of epitaxial strain on the spontaneous polarization of thin film ferroelectrics. *Phys. Rev. Lett.* **2005**, *95*, 257601.
(2) Cotrufo, M.; Sun, L.; Choi, J.; Alù, A.; Li, X. Enhancing functionalities of atomically thin semiconductors with plasmonic nanostructures. *Nanophotonics* **2019**, *8*, 577−598.
(3) Radisavljevic, B.; Kis, A. Mobility engineering and a metal−insulator transition in monolayer MoS2. *Nat. Mater.* **2013**, *12*, 815−820.
(4) Conley, H. J.; Wang, B.; Ziegler, J. I.; Haglund, R. F., Jr; Pantelides, S. T.; Bolotin, K. I. Bandgap engineering of strained monolayer and bilayer $MoS_2$. *Nano Lett.* **2013**, *13*, 3626−3630.
(5) Wang, S.; Ukhtary, M. S.; Saito, R. Strain effect on circularly polarized electroluminescence in transition metal dichalcogenides. *Phys. Rev. Res.* **2020**, *2*, 033340.
(6) Yu, T.; Wu, M. Valley depolarization dynamics and valley hall effect of excitons in monolayer and bilayer mos 2. *Phys. Rev. B* **2016**, *93*, 045414.
(7) Mohiuddin, T.; Lombardo, A.; Nair, R.; Bonetti, A.; Savini, G.; Jalil, R.; Bonini, N.; Basko, D.; Galiotis, C.; Marzari, N.; et al. Uniaxial strain in graphene by Raman spectroscopy: G peak splitting, Grüneisen parameters, and sample orientation. *Phys. Rev. B* **2009**, *79*, 205433.
(8) Desai, S. B.; Seol, G.; Kang, J. S.; Fang, H.; Battaglia, C.; Kapadia, R.; Ager, J. W.; Guo, J.; Javey, A. Strain-induced indirect to direct bandgap transition in multilayer $WSe_2$. *Nano Lett.* **2014**, *14*, 4592−4597.
(9) Wang, Y.; Cong, C.; Yang, W.; Shang, J.; Peimyoo, N.; Chen, Y.; Kang, J.; Wang, J.; Huang, W.; Yu, T. Strain-induced direct−indirect bandgap transition and phonon modulation in monolayer $WS_2$. *Nano Res.* **2015**, *8*, 2562−2572.
(10) Kumar, S.; Kaczmarczyk, A.; Gerardot, B. D. Strain-induced spatial and spectral isolation of quantum emitters in mono-and bilayer $WSe_2$. *Nano lett* **2015**, *15*, 7567−7573.
(11) Parto, K.; Azzam, S. I.; Banerjee, K.; Moody, G. Defect and strain engineering of monolayer $WSe_2$ enables site-controlled single-photon emission up to 150 K. *Nat. Commun.* **2021**, *12*, 3585.
(12) Luo, Y.; Shepard, G. D.; Ardelean, J. V.; Rhodes, D. A.; Kim, B.; Barmak, K.; Hone, J. C.; Strauf, S. Deterministic coupling of site-controlled quantum emitters in monolayer $WSe_2$ to plasmonic nanocavities. *Nat. Nanotechnol.* **2018**, *13*, 1137−1142.
(13) Wang, L.; Shih, E.-M.; Ghiotto, A.; Xian, L.; Rhodes, D. A.; Tan, C.; Claassen, M.; Kennes, D. M.; Bai, Y.; Kim, B.; et al. Correlated electronic phases in twisted bilayer transition metal dichalcogenides. *Nat. Mater.* **2020**, *19*, 861−866.
(14) Wu, F.; Lovorn, T.; Tutuc, E.; MacDonald, A. H. Hubbard model physics in transition metal dichalcogenide moiré bands. *Phys. Rev. Lett.* **2018**, *121*, 026402.
(15) Tran, K.; Moody, G.; Wu, F.; Lu, X.; Choi, J.; Kim, K.; Rai, A.; Sanchez, D. A.; Quan, J.; Singh, A.; et al. Evidence for moiré excitons in van der Waals heterostructures. *Nature* **2019**, *567*, 71−75.
(16) Singh, A.; Jo, S. S.; Li, Y.; Wu, C.; Li, M.; Jaramillo, R. Refractive uses of layered and two-dimensional materials for integrated photonics. *ACS Photonics* **2020**, *7*, 3270−3285.
(17) Sung, J.; Zhou, Y.; Scuri, G.; Zólyomi, V.; Andersen, T. I.; Yoo, H.; Wild, D. S.; Joe, A. Y.; Gelly, R. J.; Heo, H.; et al. Broken mirror symmetry in excitonic response of reconstructed domains in twisted $MoSe_2/MoSe_2$ bilayers. *Nat. Nanotechnol.* **2020**, *15*, 750−754.
(18) McGilly, L. J.; Kerelsky, A.; Finney, N. R.; Shapovalov, K.; Shih, E.-M.; Ghiotto, A.; Zeng, Y.; Moore, S. L.; Wu, W.; Bai, Y.; et al. Visualization of moiré superlattices. *Nat. Nanotechnol.* **2020**, *15*, 580−584.
(19) Andersen, T. I.; Scuri, G.; Sushko, A.; De Greve, K.; Sung, J.; Zhou, Y.; Wild, D. S.; Gelly, R. J.; Heo, H.; Bérubé, D.; et al. Excitons in a reconstructed moiré potential in twisted $WSe_2/WSe_2$ homobilayers. *Nat. Mater.* **2021**, *20*, 480−487.
(20) Bai, Y.; Zhou, L.; Wang, J.; Wu, W.; McGilly, L. J.; Halbertal, D.; Lo, C. F. B.; Liu, F.; Ardelean, J.; Rivera, P.; et al. Excitons in strain-induced one-dimensional moiré potentials at transition metal dichalcogenide heterojunctions. *Nat. Mater.* **2020**, *19*, 1068−1073.
(21) Kim, K.; Yankowitz, M.; Fallahazad, B.; Kang, S.; Movva, H. C.; Huang, S.; Larentis, S.; Corbet, C. M.; Taniguchi, T.; Watanabe, K.; et al. van der Waals heterostructures with high accuracy rotational alignment. *Nano Lett.* **2016**, *16*, 1989−1995.
(22) Lee, J.-U.; Woo, S.; Park, J.; Park, H. C.; Son, Y.-W.; Cheong, H. Strain-shear coupling in bilayer $MoS_2$. *Nat. Commun.* **2017**, *8*, 1370.
(23) Wang, Y.; Cong, C.; Qiu, C.; Yu, T. Raman spectroscopy study of lattice vibration and crystallographic orientation of monolayer $MoS_2$ under uniaxial strain. *Small* **2013**, *9*, 2857−2861.
(24) Quan, J.; Linhart, L.; Lin, M.-L.; Lee, D.; Zhu, J.; Wang, C.-Y.; Hsu, W.-T.; Choi, J.; Embley, J.; Young, C.; et al. Phonon renormalization in reconstructed $MoS_2$ moiré superlattices. *Nat. Mater.* **2021**, *20*, 1100−1105.
(25) Zhang, K.; Tadmor, E. B. Structural and electron diffraction scaling of twisted graphene bilayers. *J. Mech. Phys. Solids* **2018**, *112*, 225−238.
(26) Carr, S.; Massatt, D.; Torrisi, S. B.; Cazeaux, P.; Luskin, M.; Kaxiras, E. Relaxation and domain formation in incommensurate two-dimensional heterostructures. *Phys. Rev. B* **2018**, *98*, 224102.
(27) Alden, J. S.; Tsen, A. W.; Huang, P. Y.; Hovden, R.; Brown, L.; Park, J.; Muller, D. A.; McEuen, P. L. Strain solitons and topological defects in bilayer graphene. *Proc. Natl. Acad. Sci. U.S.A.* **2013**, *110*, 11256−11260.
(28) Nam, N. N.; Koshino, M. Lattice relaxation and energy band modulation in twisted bilayer graphene. *Phys. Rev. B* **2017**, *96*, 075311.
(29) Rosenberger, M. R.; Chuang, H.-J.; Phillips, M.; Oleshko, V. P.; McCreary, K. M.; Sivaram, S. V.; Hellberg, C. S.; Jonker, B. T. Twist Angle-Dependent Atomic Reconstruction and Moiré Patterns in Transition Metal Dichalcogenide Heterostructures. *ACS Nano* **2020**, *14*, 4550−4558.
(30) Weston, A.; Zou, Y.; Enaldiev, V.; Summerfield, A.; Clark, N.; Zólyomi, V.; Graham, A.; Yelgel, C.; Magorrian, S.; Zhou, M.; et al. Atomic reconstruction in twisted bilayers of transition metal dichalcogenides. *Nat. Nanotechnol* **2020**, *15*, 592−597.
(31) Rodríguez, Á.; Varillas, J.; Haider, G.; Kalbac, M.; Frank, O. Complex Strain Scapes in Reconstructed Transition-Metal Dichalcogenide Moire Superlattices. *ACS Nano* **2023**, *17*, 7787−7796.
(32) Cerdeira, F.; Buchenauer, C.; Pollak, F. H.; Cardona, M. Stress-induced shifts of first-order Raman frequencies of diamond-and zinc-blende-type semiconductors. *Phys. Rev. B* **1972**, *5*, 580.
(33) Li, H.; Zhang, Q.; Yap, C. C. R.; Tay, B. K.; Edwin, T. H. T.; Olivier, A.; Baillargeat, D. From bulk to monolayer $MoS_2$: evolution of Raman scattering. *Adv. Funct. Mater.* **2012**, *22*, 1385−1390.
(34) Yoo, H.; Engelke, R.; Carr, S.; Fang, S.; Zhang, K.; Cazeaux, P.; Sung, S. H.; Hovden, R.; Tsen, A. W.; Taniguchi, T.; et al. Atomic and


https://doi.org/10.1021/acs.nanolett.3c03115
*Nano Lett.* 2023, 23, 11510−11516

electronic reconstruction at the van der Waals interface in twisted bilayer graphene. *Nat. Mater.* **2019**, *18*, 448−453.
(35) Zhao, S.; Li, Z.; Huang, X.; Rupp, A.; Göser, J.; Vovk, I. A.; Kruchinin, S. Y.; Watanabe, K.; Taniguchi, T.; Bilgin, I.; et al. Excitons in mesoscopically reconstructed moiré heterostructures. *Nat. Nanotechnol.* **2023**, *18*, 572−579.



https://doi.org/10.1021/acs.nanolett.3c03115
*Nano Lett.* 2023, 23, 11510−11516